Conference paper

Chris R. Bowen*, Sam Buschhorn and Vana Adamaki

Manufacture and characterization of conductor-insulator composites based on carbon nanotubes and thermally reduced graphene oxide

Abstract: In this paper we present characterization data for carbon nanotube (CNT)-epoxy and thermally reduced graphene oxide (TRGO)-epoxy nano-composites. The frequency-dependent ac conductivity and permittivity are examined as a function of volume fraction of carbon-based filler. The measured electrical properties and their frequency dependency are evaluated on the basis that such composites can be considered as a network of resistors and capacitors, whereby the resistors represent the conductive component (CNT or TRGO) and the capacitors are the insulating component (epoxy matrix). Differences observed between the frequency-dependent electrical properties of the CNT-epoxy and TRGO-epoxy composites are explained in terms of the different electrical conductivities of the CNT and TRGO phase.

Keywords: carbon nanotubes; electrical networks; electrical properties; graphene oxide; manufacture; nano-composites; NMS-IX; permittivity.

DOI 10.1515/pac-2013-1207

Introduction

The introduction of fillers such as carbon nanotubes (CNT), graphene or thermally reduced graphene oxide (TRGO) into a polymer matrix provides numerous opportunities to tailor its electrical, thermal and mechanical properties. These composite systems are often termed electrically conductive nano-composites [1] since the introduction of a conductive carbon-based phase into an insulating polymer matrix can lead to an increase in the electrical conductivity by many orders of magnitude [2, 3], e.g., from 10^{-9} S m^{-1} up to 10 S m^{-1} or higher [3].

For CNT based composites their high aspect ratio, with a length to diameter ratio of typically 10^3–10^4 [5], favors percolation of the conductive CNT fibers through the composite system at low volume fractions; for example percolation has been observed at 0.05 vol % [4] compared to the theoretical threshold of 16 vol % for spherical particles [2, 6]. Potential applications of these high conductivity nano-composite materials include

Article note: Paper based on a presentation at the 9th International Symposium on Novel Materials and their Synthesis (NMS-IX) and the 23rd International Symposium on Fine Chemistry and Functional Polymers (FCFP-XXIII), Shanghai, China, 17–22 October 2013.

***Corresponding author: Chris R. Bowen,** Department of Mechanical Engineering, University of Bath, Bath, BA2 7AY, UK, e-mail: c.r.bowen@bath.ac.uk
Vana Adamaki: Department of Mechanical Engineering, University of Bath, Bath, BA2 7AY, UK
Sam Buschhorn: Institut für Kunststoffe und Verbundwerkstoffe – Technische Universität Hamburg-Harburg, Denickestraße 15, 21073, Hamburg, Germany

electrostatic dissipation (antistatic materials [7]), electromagnetic interference (EMI) shielding, electromagnetic absorbing materials and sensor systems.

In addition to enhanced electrical conductivity, these materials are attracting interest due to their potential 'giant' permittivity [8] where the relative permittivity of the composite can increase by three orders of magnitude relative to the matrix; such composites are reported to be of interest for applications such as high-performance capacitors [8]. This concept of an increase in effective permittivity due the addition of a conductive carbon phase contrasts with the addition of electrically insulating nanotubes, e.g., boron nitride, to a polymer which reduces the permittivity [9]. CNT based composites are by no means the optimum solution, they have the disadvantages of a tendency for the high aspect ratio nano-tubes to agglomerate during processing and the relative limited availability of large quantities of high quality material [10].

Less work has been undertaken on the electrical characterization of graphene-epoxy and reduced graphene oxide (TRGO) – epoxy composites. Graphene nano-sheets are an interesting additive material due to their two-dimensional morphology and exceptional electrical, mechanical and thermal properties along with the relative abundance of the graphite precursor material. Graphene based polymer nano-composites have been considered for applications [10] such as sensors, electro-static discharge materials, electromagnetic shielding [11] and electrodes. Graphene nano-composites can exhibit superior mechanical properties compared to the host polymer matrix, high thermal stability, thermal conductivity and electrical conductivity [12]. A variety of methods have been employed to form graphene nano-sheets and thermal exfoliation of graphite oxide (GO) coupled with in situ reduction is currently a popular route to produce graphene nano-sheets in relatively large quantities [13]. The presence of oxygen-containing groups is also thought to facilitate the dispersion of the nanosheets in polar polymers [14]. As an example, polystyrene/graphene nano-composites exhibited a percolation threshold as low as 0.1 vol % [12, 15] and PET/graphene attained an electrical conductivity of 3.3×10^{-5} S/m at 0.56 vol % loading; this is higher than the antistatic criterion of 10^{-6} S/m [13].

This paper describes the manufacture of both CNT-epoxy and TRGO-epoxy nano-composites and examines the frequency dependent properties of the carbon based nano-composites. Differences between the CNT-epoxy and TRGO-epoxy composites are examined with respect to the frequency dependence of parameters such as ac conductivity, permittivity, phase angle and loss tangent (tan δ). A simple approach to understand the frequency dependence of properties is discussed in terms of considering the carbon-epoxy composite as a resistor-capacitor network.

Experimental

CNT and TRGO epoxy nano-composites

Multiwall carbon nanotubes grown by chemical vapor deposition were supplied by Bayer Material Science ('Baytubes C150P'). The nanotubes typically have average inner and outer diameters of ~4 and ~13 nm, respectively [16]. The CNT length is 1–4 μm [16]. The matrix was a LY556 Bisphenol A based resin from Huntsman with the curing agents Araldite 917 and DY 070 in the recommended proportions [17].

The filler was incorporated in the resin and dispersed using a three-roll mill high shear dispersion system (EXAKT 120 E, EXAKT Advanced Technologies GmbH, Germany). Adjacent roll surfaces have a different rotational speed which ensure a thorough dispersion of particles in the resin. The use of a decreasing gap size between the rolls and repeating the process several times with a final gap size of 5 μm with shear rates in excess of 10^7 m s^{-1} allows a repeatable and high degree of exfoliation of the nano-particles into the resin.

This dispersion was then mixed with the hardener and accelerator, then cured in a mold following the recommended cycle with a maximum temperature of 140 °C. The plate that is produced is a few mm thick and 80 mm × 100 mm wide. Samples taken from different locations have similar properties if approximately 50 μm of edge material is ground off with 400 grit abrasive paper. Final sample sizes were 10 mm × 10 mm with an approximate thickness of 1 mm between two silver paint electrodes.

The production of the GO is given in detail in [18] and the GO has been thermally reduced to improve the electrical conductivity. Details of the reduction process for the TRGO is described in detail in [19]. Further processing is done analogous to the carbon nanotube samples to form the nano-composites.

Impedance measurements

The ac conductivity (admittance) was calculated using eq. 1,

$$\sigma = \frac{Z'}{Z'^2 + Z''^2} \cdot \frac{t}{A}. \tag{1}$$

where Z' and Z'' are the real and imaginary parts of the impedance, A is the area of the sample and t is the sample thickness. The real part of the relative permittivity (dielectric constant) was calculated using eq. 2,

$$\varepsilon = \frac{-Z''}{Z'^2 + Z''^2} \cdot \frac{t}{\omega \cdot A \cdot \varepsilon_0} \tag{2}$$

where ω is the angular frequency ($2\pi f$), f is frequency and ε_0 is the permittivity of free space. The phase angle (θ) between current and voltage and loss tangent (tan δ) was determined from eq. 3 and eq. 4 respectively.

$$\theta = \tan^{-1}(Z'' / Z') \tag{3}$$

$$\tan\delta = (Z' / Z'') \tag{4}$$

Results and discussion

Background to R-C networks of relevance to carbon-epoxy composites

Before discussing the electrical properties of CNT-epoxy and TRGO-epoxy nano-composite systems it is of interest to initially discuss the electrical response of composite systems in the context of resistor-capacitor networks. Heterogeneous materials that contain conductive and insulating phases are present in ceramics, polymers and the carbon-based nano-composites studied here. These materials often exhibit a very similar frequency-dependent conductivity and permittivity, often termed Jonscher's "universal dielectric response" (UDR) [20]. A characteristic of the UDR is that at low frequencies the bulk ac conductivity is frequency independent, σ_{dc}, while at higher frequencies the ac conductivity increases following a power law behavior namely,

$$\sigma(\omega) = \sigma_{dc} + A\omega^n \tag{5}$$

where A is a constant and $0 < n < 1$. The relative permittivity (ε) can also be described by a power-law decay [20, 21],

$$\varepsilon(\omega) \propto \omega^{n-1} \tag{6}$$

Previous work [22, 23] has shown that a large network of resistors (R) and capacitors (C) can simulate a composite consisting of a random distribution of regions that are conductors (resistors) and insulators (capacitors). The networks exhibit fractional power law frequency dependences of ac conductivity and permittivity which are remarkably similar to eqs. 1 and 2. Observations from the study of R-C networks [22–24] were:

(i) at low frequencies, where $R^{-1} > \omega C$, currents flow preferentially through the resistors,
(ii) at high frequencies, where $R^{-1} < \omega C$, currents flow preferentially through the capacitors,

(iii) at intermediate frequencies, where $R^{-1} \sim \omega C$, currents flow through both R and C,
(iv) power law dependencies are observed in the frequency range where currents flow through both resistors and capacitors; i.e., when $R^{-1} \sim \omega C$.

The power law response of the network has been observed to be related to the resistor and capacitor values by a logarithmic mixing rule where the complex conductivity of the network ($\sigma^*_{network}$) could be described as, $\sigma^*_{network} = (i\omega C)^{\alpha}(R^{-1})^{1-\alpha}$, where α is the fraction of capacitors. Based on the logarithmic mixing rule above, a random mixture of conductive and insulating phases was found to follow eq. 3 and 4 below,

$$\sigma_{composite} = (\omega\varepsilon\varepsilon_0)^{\alpha}(\sigma)^{1-\alpha}\cos\left(\frac{\alpha\pi}{n}\right) \tag{7}$$

$$\varepsilon_{composite} = (\omega\varepsilon_0)^{\alpha-1}(\varepsilon)^{\alpha}(\sigma)^{1-\alpha}\sin\left(\frac{\alpha\pi}{n}\right) \tag{8}$$

where σ is the conductivity of the conducting phase (CNT or TRGO in this work), ε is the relative permittivity of the insulating phase (polymer matrix) and α is the fractional volume of the material occupied by the insulating phase. Equations 3 and 4 predict that the power law exponent (n) in the UDR (eqs. 1 and 2) is related to the fractional volumes of the conducting ($1–\alpha$) and insulating (α) regions in a material at the condition where $\sigma \sim \omega\varepsilon\varepsilon_0$. This R-C approach to understand ac properties has been used to describe the frequency dependent electrical properties of a range of carbons in a polymer matrix such as carbon black [24], multi-walled CNTs [26] and CNTs [27, 28]; including the use of more complex electrical networks comprised of resistors, capacitors and diodes (an R-C-D network) [27].

Finally, it is of interest to note that at the condition $\sigma \sim \omega\varepsilon\varepsilon_0$ the electrical response of the network is independent of the precise arrangement of resistors and capacitors since ac currents are flowing through *both* components. This is in contrast to the low frequency (dc) condition where the network response is highly sensitive to the arrangement of resistors (percolation paths); this is one potential reason why low frequency properties may vary between individual samples or are highly dependent on processing conditions for large surface area nanoparticles.

CNT-epoxy composites

Figure 1 shows a high-magnification scanning electron microscopy (SEM) micrograph of a cryofracture surface of the cured CNT-epoxy material. Bright spots represent carbon nanotubes pulled out of the surface or nanotubes that are still embedded in epoxy close to the surface of the fracture. The nanotubes are well exfoliated, but their distribution is not completely homogeneous. This is typically the case when the matrix allows for some re-agglomeration, e.g., through low viscosity in the initial stage of curing.

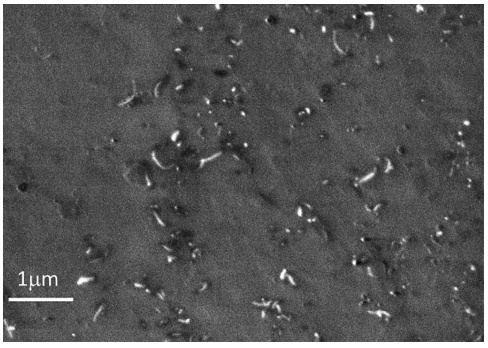

Fig. 1 Scanning electron microscopy image of cryofracture of 0.3 wt % CNT – epoxy composite.

Figure 2a shows the frequency dependency of the real part of the complex conductivity of the CNT-epoxy composites for a variety of CNT loadings (0 to 0.6 wt %). The conductivity of the pure epoxy material (LY556) rises linearly with frequency and in this case the fraction of capacitors (α) in eq. 3 can be considered to be unity so that $\sigma(\omega) = \omega\varepsilon_{epoxy}\varepsilon_0$; this is typical of a highly insulating material (dielectric) [2].

As a small amount of CNT is added to the epoxy (e.g., 0.05 wt %) the low frequency conductivity, σ_{dc}, at ~10 Hz in Fig. 2a rises by over six orders of magnitude. In addition to increasing in magnitude, the conductivity becomes almost frequency independent across the whole frequency range studied here. Greater additions of CNT lead to the conductivity continuing to increase, although the rate of increase is smaller with increasing CNT content; for example the increase is less than an order of magnitude for CNT additions of 0.3 wt % to 0.6 wt %.

This immediate transition from a frequency dependent conductivity at 0 wt % to a frequency independent conductivity at low CNT weight fractions of 0.05 wt % (and above) is a result of the high electrical conductivity of the CNT nanotubes combined with their pronounced tendency to percolate to create conductive paths across the nano-composite structure. The electrical conductivity of the C150P carbon nanotubes (σ_{C150P}) is reported to be as high as 10^6 S/m [29] and indirect methods have measured a conductivity of 3981 S/m [30]. The measured relative permittivity of the epoxy is $\varepsilon_{epoxy} \sim 5$ (see Fig. 2b). If we consider the CNT-epoxy system as a network of resistors of conductivity σ_{C150P} and capacitors of permittivity ε_{epoxy} then $\sigma_{C150P} >> 2\pi.f.\varepsilon_{epoxy}.\varepsilon_0$ for the frequencies examined in

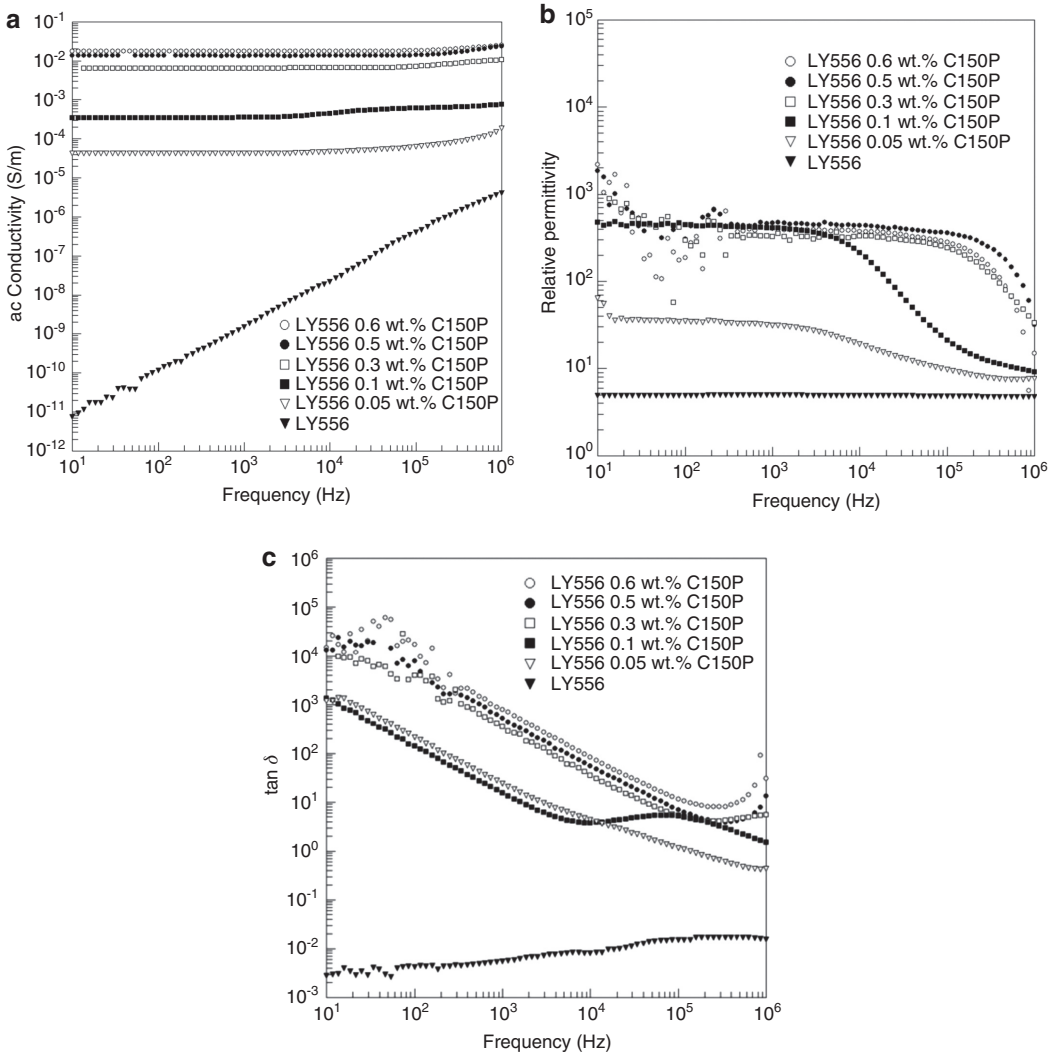

Fig. 2 (a) ac conductivity, (b) relative permittivity and (c) tan δ as a function of frequency for CNT – epoxy composites.

this work (less than 10^6 Hz). Based on such a high electrical conductivity and the CNT, UDR behavior of the type in eq. 1 would only be observed at much higher frequencies (in excess of 10 THz); for example Nuzhyy et al. [31] observed the UDR on CNT-polymer composites by characterization up to THz frequencies.

Figure 2b shows the frequency dependent relative permittivity of the CNT-epoxy nano-composites for the same range of CNT volume fractions. The pure epoxy (LY556) has a constant relative permittivity as a function of frequency at ~5, as would be expected for a dielectric phase and corresponds to the fraction of capacitors (α) being unity in eq. 8 and the permittivity being frequency independent. As CNTs are added to the epoxy the relative permittivity rises, especially at low frequencies (less than 1 kHz), and increases from a ~5 for the pure epoxy to ~500 for CNT fractions of 0.1 wt % and above. Similar behavior was reported by Yuan et al. [8] on CNT dispersed in a polyvinylidene fluoride (PVDF) matrix who suggested this is due to the percolated network consisting of CNTs that are almost touching each other but remain electrically insulated. Pötschke et al. [5, 32] and Liang et al. [33] also observed a similar decrease in the real part of the permittivity with frequency.

In many systems the addition of a conductive filler to an insulating matrix leads to a permittivity that decreases with increasing frequency. However in this system the permittivity is frequency independent up to relatively high frequencies (<10^3 Hz), see Fig. 2b. At low frequencies conductive paths flow preferentially through the conductive CNT filler since $\sigma_{C150P} >> 2\pi.f.\varepsilon_{epoxy}.\varepsilon_0$ and the high effective permittivity is thought to be a result of small regions of insulating matrix between the conductive regions. Jiang et al. [34] describe these regions as one in which the CNTs are separated by a small layer of polymer and can be regarded as a series of 'micro-capacitors' which allows the composite to store charge. The frequency independence of permittivity at low frequencies is a result of the high conductivity of the CNT additions ($\sigma_{C150P} >> 2\pi.f.\varepsilon_{epoxy}.\varepsilon_0$) and ac currents continue to flow preferentially through the CNT phase for frequencies up to 10^3 Hz and the effective permittivity remains constant and high due to the 'micro-capacitor' regions. As the frequency rises the ac conductivity of the dielectric phase ($2\pi.f.\varepsilon_{epoxy}.\varepsilon_0$) rises and the permittivity is no longer dominated by the 'micro-capacitor' regions. This leads to the effective permittivity decreasing with increasing frequency which, at a sufficiently high frequency, will approach the permittivity values of the pure LY556 material (see Fig. 2b).

The high dielectric constant at low frequency may initially appear attractive for applications such as volume efficient capacitors, however since the nano-composite consists of thin regions of polymer separated by conductive material there is a reduction in electrical breakdown strength [25].

The variation of tan δ (loss tangent) with frequency for the CNT-epoxy composites is shown in Fig. 2c. For the pure epoxy matrix tan δ is low in magnitude (10^{-2}–10^{-3}) and almost frequency independent; consistent with the material behaving as a dielectric. As CNTs are added to the epoxy the loss tangent rises significantly (e.g., 10^3 at 10 Hz for 0.05 wt %) and becomes frequency dependent. The frequency dependency arises since the loss tangent is the ratio of the real to imaginary permittivity (eq. 4) and the contribution of conductivity to the loss tangent is larger at low frequencies where the current flow occurs preferentially through the conductive phase (the resistors in the R-C network) [35].

Figure 3 shows complex plane impedance diagrams, namely real (Z′) versus imaginary (Z″) impedance for CNT-epoxy nano-composites for different CNT volume fractions (0.05 wt %, 0.3 wt %. 0.5 wt %, 0.6 wt %), where the impedance values have been normalized with respect to sample geometry (area and thickness). For the pure epoxy the response is purely capacitive and therefore no semi-circle is observed since there is no real component and Z′~0 (data not shown). From Fig. 3 it can be observed that as CNTs are added to the epoxy the introduction of real component to the impedance leads to the formation a semi-circle which is typical of a parallel RC circuit [36]. The low frequency intercept on the Z′ axis (maximum value of Z′) corresponds to the resistivity of the sample and gradually decreases as CNT fraction increases (compare Fig. 3a to 3d). The maximum value of the imaginary component also decreases with increasing CNT.

TRGO-epoxy composites

Figure 4 shows an SEM micrograph of a cryofracture surface of an intermediate product in the cured form. Here the dispersion is deliberately not completed, as the achievable contrast is generally too low for a mean-

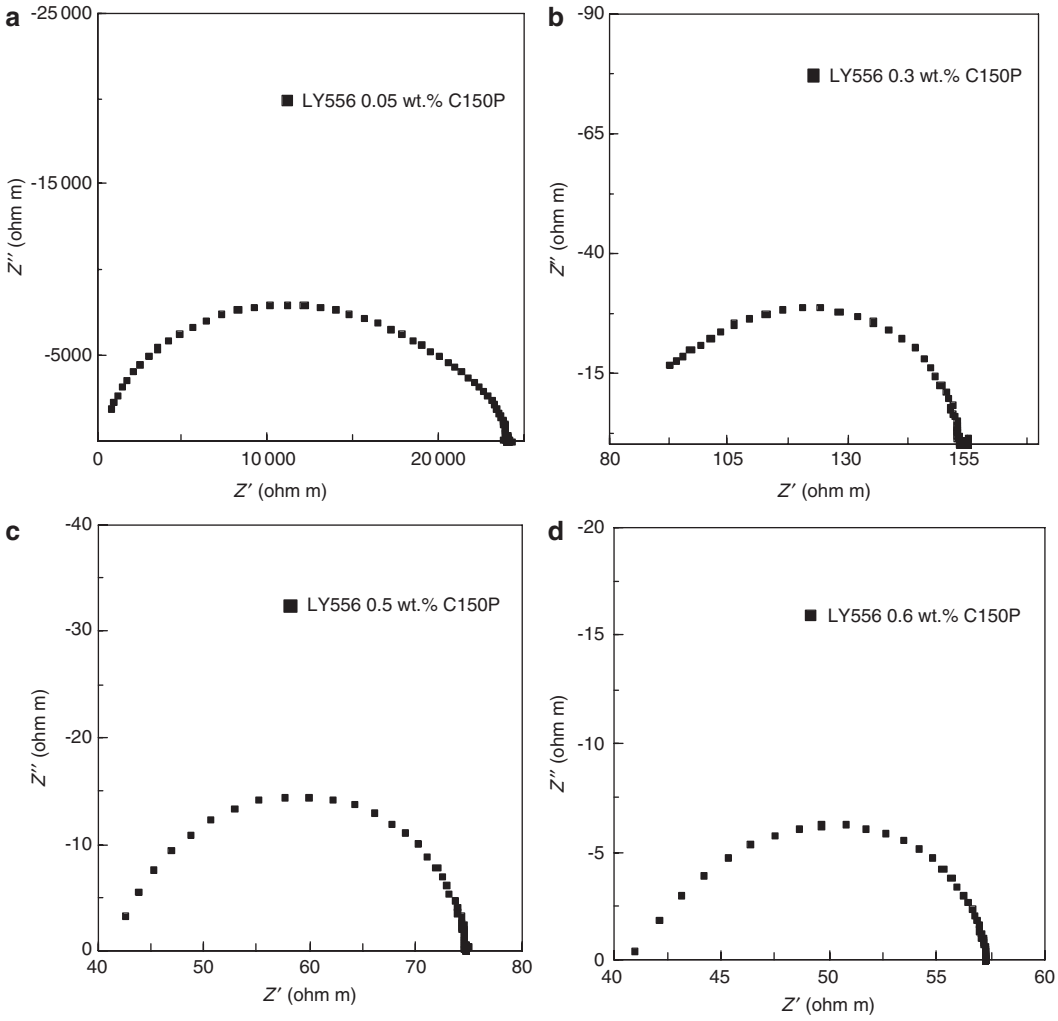

Fig. 3 Real and imaginary impedance for CNT-epoxy composites with (a) 0.05 wt % CNT (b) 0.3 wt % CNT (c) 0.5 wt% CNT (d) 0.6 wt % CNT.

ingful image of the final product. However, even after the initial stages of dispersion a good distribution of carbon particles, visible as bright specks, is observed. The bright contour lines are due to the fracture surface and cannot be directly attributed to the immediate presence of TRGO.

Figure 5 shows the ac conductivity as a function of frequency for the TRGO-epoxy nano-composites. The pure epoxy matrix exhibits a low conductivity which rises linearly with frequency. As TRGO is added to

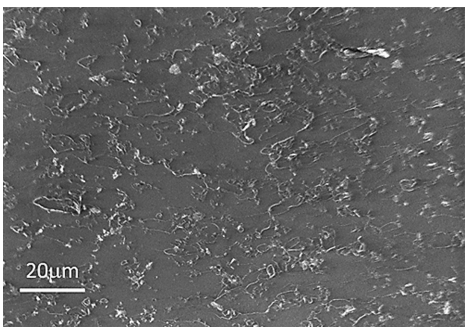

Fig. 4 Scanning electron microscopy image cryofracture of a 0.3 wt % TRGO-epoxy composite.

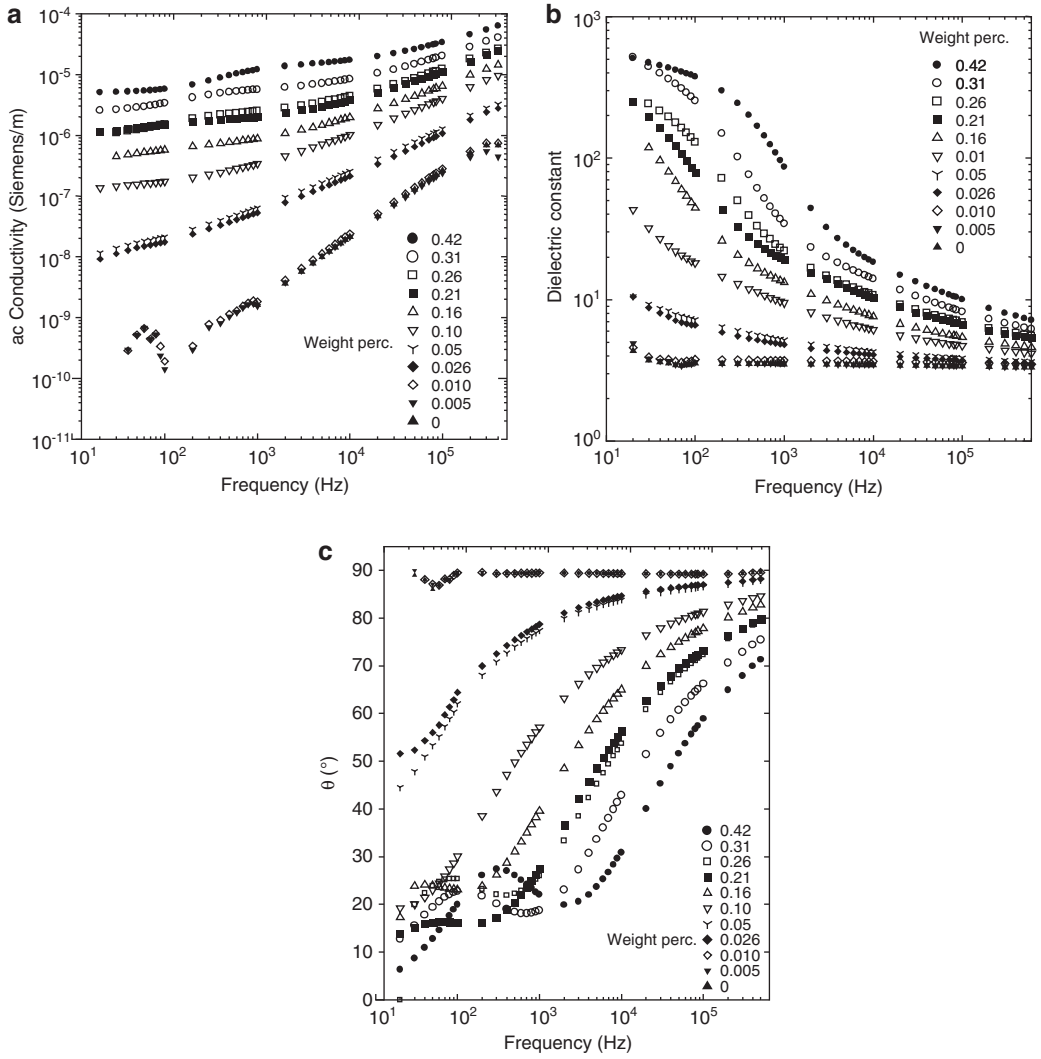

Fig. 5 (a) ac conductivity, (b) relative permittivity and (c) phase angle as a function of frequency for thermally reduced graphene oxide – epoxy composites.

the matrix the low frequency conductivity begins to rise; the increase is smaller compared to the CNT-epoxy system (compare Fig. 2a and 5a). The TRGO-epoxy composites in which the weight fractions are in excess of 0.1 wt % exhibit typical UDR behavior, i.e., at low frequencies the bulk ac conductivity is frequency independent while at higher frequencies the ac conductivity increases following a power law. In this case the TRGO has a lower conductivity than the CNT; for example reported values are in the range of 6×10^{-5} S/m to 20 S/m [37] so that the condition $\sigma_{\mathrm{TRGO}} \sim 2\pi f \varepsilon_{\mathrm{epoxy}} \varepsilon_0$ is achieved within the frequency range studied (e.g., 200 kHz for a conductivity of 6×10^{-5} S/m). Figure 5b shows the variation of dielectric constant (relative permittivity) as a function of frequency. For the pure epoxy material, the dielectric constant is almost frequency independent and as TRGO is gradually added to the matrix the composites exhibits UDR in that the dielectric constant is high at low frequency and then falls with increasing frequency. In contrast to the CNT composites (Fig. 2b), the dielectric constant of the TRGO-composites decreases with increasing frequency for the frequency range examined; this is due to the lower conductivity of the TRGO compared to the CNT composites. At high frequencies (>10^5 Hz) the dielectric constant approaches the same value and is less dependent on TRGO content; this is a consequence of the ac current paths including the insulating epoxy phase to a larger degree and is analogous to the condition $R^{-1} \sim \omega C$ in the R-C network. This transition from currents flowing through the conductive component at low frequency ($R^{-1} > \omega C$) to currents flowing through both conductive and insulating

phases at $R^{-1} \sim \omega C$ can be seen by examination of the variation of phase angle with frequency (Fig. 5c). For the epoxy material the phase angle between current and voltage is 90° since the material is insulating and behaving purely as a capacitor. As TRGO is added the phase angle approaches zero, especially for the composites in excess of 0.1 wt % at low frequency (less than 10^2 Hz). As the frequency increases and $2\pi f\varepsilon_{epoxy}\varepsilon_0$ rises and approaches σ_{TRGO} currents begin to flow through the capacitative phase and the phase angle begins to return to 90°; see the phase angle at frequencies greater than 10^5 Hz in Fig. 5c.

Conclusions

This paper has undertaken the manufacture and characterization of the frequency dependent conductivity and permittivity of CNT-epoxy and TRGO-epoxy nano-composites and discussed their behavior in terms of a simple R-C electrical network. For the CNT-epoxy system the initially dielectric epoxy exhibits a frequency dependent conductivity, $\sigma(\omega) = \omega\varepsilon_{epoxy}\varepsilon_0$. Since $\sigma_{C150P} >> 2\pi f\varepsilon_{epoxy}\varepsilon_0$ the addition of percolated and high conductivity CNTs to the epoxy results in a rapid transition to purely conductive behavior with a frequency independent conductivity. Electrical conductivities of the order of 10^{-2} S/m were achieved for additions of 0.3 wt % to the epoxy matrix. For the TRGO-epoxy system the lower electrical conductivity leads to a more gradual change in electrical properties. Additions of approximately 0.3 wt % TRGO led to a low frequency electrical conductivity of the order of 10^{-5}–10^{-6} S/m. In contrast to the CNT-epoxy system, the TRGO-epoxy composites exhibit UDR behavior and a frequency dependent ac conductivity and permittivity. At low frequencies the TRGO loaded epoxies have a frequency independent conductivity since currents flow preferentially through the conductive TRGO phase. As the frequency increases and $\sigma_{GO} \sim 2\pi f\varepsilon_{epoxy}\varepsilon_0$ ac current paths include the insulating epoxy phase leading to the ac conductivity rising with frequency and permittivity falling with frequency; this is also observed in the phase angle which changes from low values at low frequency (restive behavior) to 90° at higher frequencies. The R-C network provides an insight to the variation of properties such as conductivity, permittivity, loss and phase angle which frequency and provides a simple approach to understand requirements to tune the frequency dependent properties of carbon-epoxy nano-composites for specific applications.

Acknowledgments: We acknowledge Prof. Mülhaupt from the University of Freiburg for providing the thermally reduced graphene oxide. Chris Bowen acknowledges funding from the European Research Council under the European Union's Seventh Framework Programme (FP/2007-2013) / ERC Grant Agreement no. 320963 on Novel Energy Materials, Engineering Science and Integrated Systems (NEMESIS).

References

[1] E. Logakis, P. Pissis, D. Pospiech, A. Korwitz, B. Krause, U. Reuter, P. Pötschke. *Euro. Polym. J.* **46**, 928 (2010).
[2] C. A. Martin, J. K. W. Sandler, M. S. P. Shaffer, M. K. Schwarz, W. Bauhofer, K. Schulte, A. H. Windle. *Comp. Sci. Tech*. **64**, 2309 (2004).
[3] E. Logakis, Ch. Pandis, V. Peoglas, P. Pissis, J. Pionteck, P. Pötschke, M. Mičušik, M. Omastová. *Polymer* **50**, 5103 (2009).
[4] I. Alig, D. Lellinger, S. M. Dudkin, P. Pötschke. *Polymer* **48**, 1020 (2007).
[5] P. Pötschke, M. Abdel-Goad, I. Alig, S. Dudkin, D. Lellinger. *Polymer* **45**, 8863 (2004).
[6] S. Kirkpatrick. *Rev. Mod. Phys*. **45**, 574 (1973).
[7] S. Barrau, P. Demont, A. Peigney, C. Laurent, C. Lacabanne. *Macromolecules* **36**, 5187 (2003).
[8] J. K. Yuan, S. H. Yao, Z. M. Dang, A. Sylvestre, M. Genestoux, J. Bai. *J. Phys. Chem. C*. **115**, 5515 (2011).
[9] C. Y. Zhi, Y. Bando, T. Terao, C. Tang, D. Golberg. *Pure. Appl. Chem*. **82**, 2175 (2010).
[10] R. Verdejo, M. M. Bernal, L. J. Romasanta, M. A. Lopez-Manchado. *J. Mater. Chem*. **21**, 3301 (2011).
[11] J. Lang, Y. Wang, Y. Huang, Y. Ma, Z. Liu, J. Cai, C. Zhang, H. Gao, Y. Chen. *Carbon* **47**, 922 (2009).
[12] T. Kuilla, S. Bhadra, D. Yao, N. H. Kim, S. Bose, J. H. Lee. *Prog. Poly. Sci.* **35**, 1350 (2010).
[13] H. B. Zhang, W. G. Zheng, Q. Yan, Y. Yang, J. W. Wang, Z. H. Lu, G. Y. Ji, Z. Z. Yu. *Polymer* **51**, 1191 (2010).

[14] T. Ramanathan, A. A. Abdala, S. Stankovich, D. A. Dikin, M. Herrera-Alonso, R. D. Piner, D. H. Adamson, H. C. Schniepp, X. Chen, R. S. Ruoff, S. T. Nguyen, I. A. Aksay, R. K. Prud'Homme, L. C. Brinson. *Nature Nanotechnology* **3**, 327 (2008).
[15] S. Stankovich, D. A. Dikin, G. H. B. Dommett, K. M. Kohlhaas, E. J. Zimney, E. A. Stach, R. D. Piner, S. T. Nguyen, R. S. Ruoff. *Nature* **442**, 282 (2005).
[16] J. O. Aguilar, J. R. Bautista-Quijano, F. Avilés. *Express Poly. Lett.* **4**, 292 (2010).
[17] S. C. Schulz, G. Faiella, S. T. Buschhorn, K. Schulte, M. Giordano, W. Bauhofer. *Annual Transactions of the Nordic Rheology Society* **19**, 1 (2011).
[18] P. Steurer, R. Wissert, R. Thomann, R. Mülhaupt. *Macromol. Rapid Commun*. **30**, 316 (2009).
[19] S. Chandrasekaran, G. Faiella, L. A. S. A. Prado, F. Tölle, R. Mülhaupt, K. Schulte. *Composites: Part A.* **49**, 51 (2013).
[20] A. K. Jonscher. *Nature* **267**, 673 (1977).
[21] C. Brosseau, P. Quéffélec, P. Talbot. *J. App. Phys.* **89**, 4532 (2001).
[22] D. P. Almond, B. Vainas. *J. Phys. Condens. Matter* **11**, 9081 (1999).
[23] D. P. Almond, C. R. Bowen. *Phys. Rev. Lett.* **92**, 157601 (2004).
[24] D. P. Almond, C. R. Bowen, D. A. S. Rees. *J. Phys. D: Appl. Phys*. **39**, 1295 (2006).
[25] H. Stoyanov, D. Mc Carthy, M. Kollosche, G. Kofod. *App. Phys. Lett.* **94**, 232905 (2009).
[26] P. K. Mural, G. Madras, S. Bose, *RSC Adv*. **4**, 4943 (2014).
[27] D. S. Bychanok, A. G. Paddubskaya, P. P. Kuzhir, S. A. Maksimenko, C. Brosseau, J. Macutkevic, S. Bellucci. arXiv:1311.3479 (2013).
[28] S. Pfeifer, S. H. Park, P. R. Bandaru. *ECS Solid State Lett.* **2**, M5 (2013).
[29] Baytubes, Multi-Walled Nanotubes, Preliminary Datasheet for Product Development, Bayer Materials Science AG, Germany (2005).
[30] I. D. Rosca, S. V. Hoa. *Carbon* **47**, 1958 (2009).
[31] D. Nuzhnyy, M. Savinov, V. Bovtun, M. Kempa, J. Petzelt, B. Mayoral, T. McNally. *Nanotechnology* **24**, 055707 (2013).
[32] P. Pötschke, S. M. Dudkin, I. Alig. *Polymer* **44**, 5023 (2003).
[33] G. D. Liang, S. C. Tjong. *Mat. Chem. Phys*. **100**, 132 (2006).
[34] M. J. Jiang, Z. M. Dang, M. Bozlar, F. Miomandre, J. Bai. *J. App. Phys.* **106**, 084902 (2009).
[35] D. A. Robinson, S. B. Jones, J. M. Wraith, D. Or, S. P. Friedman. *Vadose Zone J.* **2**, 444 (2003).
[36] W. K. Hsu, V. Kotzeva, P. C. P. Watts, G. Z. Chen. *Carbon* **42**, 1707 (2004).
[37] T. Kuila, P. Khanra, S. Bose, N. H. Kim, B. C. Ku, B. Moon, J. H. Lee. *Nanotechnology* **22**, 305710 (2011).